Supplementary Information (SI) for Journal of Materials Chemistry A.

Supplementary Information

Boosting the ORR Activity in PEM Fuel Cell: Tailored Electron-Withdrawing Properties of Fe-Based Catalysts via Optimizing Fluorine Doping

Nan Xue[a,b], Jian Yin[a], Xueyan Xue[a,b], Hui Zhu[a*], Jiao Yin[a*]

[a] Laboratory of Environmental Sciences and Technology, Xinjiang Technical Institute of Physics & Chemistry, and Key Laboratory of Functional Materials and Devices for Special Environments, Chinese Academy of Sciences, Urumqi 830011, China

[b] University of Chinese Academy of Sciences, Beijing 100049, China

Corresponding author:

huizhu@ms.xjb.ac.cn (H. Zhu); yinjiao@ms.xjb.ac.cn (J. Yin)

Experimental and methods

Materials

Iron nitrate nonahydrate ($Fe(NO_3)_2 \cdot 9H_2O$), Zinc nitrate hexahydrate ($Zn(NO_3)_2 \cdot 6H_2O$) and 2-methylimidazole, tetrafluoroterephthalic acid (TFTP) were purchased from Aladdin. Perchloric acid, Methanol, Ethanol and Iso-Propyl Alcohol (IPA) were ordered from Sinopharm Chemical. Commercial Pt/C (20 %) was obtained from Adamas. Nafion (5 %) was purchased from Aldrich. The deionized (DI) water employed was obtained through RO system. All chemicals were from commercial and used without further purification.

Catalyst synthesis

Preparation of Fe-N/F-CNT and Fe-N-CNT catalyst. In a typical synthesis, 0.1 mmol $Fe(NO_3)_2 \cdot 9H_2O$, and 2 mmol $Zn(NO_3)_2 \cdot 6H_2O$ were dissolved in 100 mL of methanol and named solution A. Then 8 mmol 2-methylimidazole and 600 mg TFTP were added into 100ml methanol and fully stirred and dispersed, named solution B. After that, the solution A and solution B were mixed and vigorously stirred at room temperature for 24h. The as-obtained precipitates were centrifuged and washed with methanol several times and dried in vacuum at 60 ˚C for overnight. The above precursor was rapidly heated up to 1000 °C in argon for 30 min, annealed for 1 h and then naturally cooled to room temperature to obtain the Fe-N/F-CNT-2 catalyst. For comparison, Fe-N/F-CNT-1 and Fe-N/F-CNT-3 samples were prepared with 400 mg and 800mg TFTP, respectively. In addition, Fe-N-CNT samples were prepared by the same method, but without the use of TFTP.

Characterizations

The X-ray diffraction (XRD) was acquired on a Bruker D8 Advance, scanning from $2\theta=10^{\circ}$-80°. SEM images and EDS elemental mappings were recorded using a Philips XL 30 instrument and a JEOL JSM-6700F microscope. TEM images were taken on FEI Tecnai G2 F20 transmission electron microscope with an acceleration voltage of 200 kV. XPS was measured with an ESCALAB250 (Thermo Electron). The X-ray excitation was provided by a monochromatic Al $K\alpha$ (1486.6eV) source. Data quantification was performed on the Avantage program. The surface atomic concentrations were determined from photoelectron peaks areas using the atomic sensitivity factors reported by Scofield. Binding energies of all core levels were referred to the C-C bond of C1s at 284.6 eV. Raman spectra were measured with a Raman microspectrometer (LabRAM HR Evolution-HORIBA Scientific) using an Ar^+ laser (100 mW, 532 nm) as excitation source and measured using a microscope equipped with a 50×objective. Nitrogen adsorption/desorption isotherms were measured at 77 K with Quantachrome adsorption instrument. The surface area was calculated according to the Brunauer-Emmett-Teller (BET) method. Fourier transform infrared spectra (FITR) were collected in an infrared spectrometer (NICOLET Is50 FT-IR, Thermo Scientific). XG-CAMA contact angle system was employed to determine the catalysts hydrophobicity.

Electrochemical measurements

5mg of Fe-N/F-CNT-1, Fe-N/F-CNT-2, Fe-N/F-CNT-3 and Fe-N-CNT were ultrasonically dispersed in a mixed solution of 360 µL ethanol, 120 µL H_2O and 20 µL 5 wt % Nafion for 30 minutes to prepare suspension. Take 10µL of the suspension and transfer it onto a glassy carbon disk (Φ = 5 mm) with a loading of 0.51 mg cm^{-2}. While, commercial Pt/C (20 %) sample was prepared by dispersing 5 mg of the catalyst in 1 mL of solution the loading of Pt/C was 0.051 mg_{Pt} cm^{-1}.

All electrochemical experiments were conducted on a CHI760E electrochemical station. Gaphite rod was used as the counter electrode and Ag/AgCl was utilized as the reference electrode. Prior to measurement, electrode O_2 or N_2 was passed into the 0.1M $HClO_4$ solution for 30 minutes to saturate the electrolyte. Cyclic voltammetry (CV) curves were recorded at a scan rate of 50mV s^{-1}. Linear sweep voltammetry (LSV) test was performed at a range of 0.1 to 1 V (vs. RHE) at a scan rate of 10 mV s^{-1}, where the disk electrode speed was 1600 rpm.

The yield of H_2O_2 and the number of electron transfers n are calculated from the RRDE measurement by the following equations:

$$H_2O_2\,(\%) = \frac{200 \times I_r}{I_d N + I_r} \qquad (1)$$

$$n = \frac{4 I_d N}{I_d N + I_r} \qquad (2)$$

where, I_d and I_r represent the disk current and the ring current, respectively, and the collection efficiency of ring electrode N is 0.37.

In situ electrochemical measurements of Fe-Nx active sites were performed using the nitrite stripping experiment proposed by Malko et al.[1] Briefly, an acetate buffer of 0.5 M with pH 5.2 was prepared from sodium acetate and acetic acid. The CV was carried out between 1.05 to -0.4V vs. RHE in alternative N_2 and O_2-saturated 0.5 M acetate buffer electrolyte. This was repeated until reaching steady-state CV data. Before and after being poisoned by $NaNO_2$ poisoning procedure, CV curves were recorded between 0.4 and -0.3 V vs. RHE in a N_2-saturated. The site density (SD) can be calculated according to the following formulas:[2]

$$SD = \frac{Q_{\mathrm{strip}} \times N_A}{n_{\mathrm{strip}} F} \qquad (3)$$

where Q strip (C g^{-1}) is the reduction charge of nitrite, n_{strip} is the number of electrons associated with the reduction of one adsorbed nitrosyl per site and its value is 5, N_A is Avogadro's constant (mol^{-1}) and F is Faraday's constant (C mol^{-1}).

MEA preparation and fuel cell test

The membrane electrode assembly (MEA) was prepared through catalyst-coated membranes (CCM). Fe-N/F-CNT-2 or Fe-N-CNT catalyst was employed as the cathode catalyst, commercial Pt/C (20 wt%) was used as the anode catalyst to prepare the catalyst ink. Nafion 211 membrane of DuPont in the United States was used as the proton exchange membrane, and the carbon paper of Toray in Japan was used as the gas diffusion layers (GDL). The cathode catalyst load was 4.0 mg cm^{-2} and the Pt loading in the cathode was 0.1 mg_{Pt} cm^{-2}. Then, the cathode and anode catalyst inks were respectively coated on both sides of Nafion 211 membrane to form CCM. Finally, the CCM and GDL were stacked together and heat-pressed to form MEA. The active area of MEA was 2 × 2 cm^2. The fuel cell performance was tested in a single cell test system with a direct parallel flow path. H_2 humidified at 80 °C provide gas to the anode and cathode of the fuel cell at a flow rate of 200 mL min^{-1} and 200 mL min^{-1}, respectively. The fuel cell polarization curves were recorded at 80 °C, 1 bar back pressure.

Density Functional Theory (DFT) calculations

We have employed the first-principles[3, 4] to perform density functional theory (DFT) calculations within the generalized gradient approximation (GGA) using the Perdew-Burke-Ernzerhof (PBE)[5] formulation. We have chosen the projected augmented wave (PAW) potentials[6, 7] to describe the ionic cores and take valence electrons into account using a plane wave basis set with a kinetic energy cutoff of 500 eV. Partial occupancies of the Kohn−Sham orbitals were allowed using the Gaussian smearing method with a width of 0.05 eV. The electronic energy was considered self-consistent when the energy change was smaller than 10^{-5} eV. A geometry optimization was considered convergent when the energy change was smaller than 0.05 eV $Å^{-1}$. The Brillouin zone integration is performed using 2×2×1 Monkhorst-Pack k-point sampling for a structure. Finally, the adsorption energies (E_{ads}) were calculated as $E_{ads}= E_{ad/sub} - E_{ad} - E_{sub}$, where $E_{ad/sub}$, E_{ad}, and E_{sub} are the total energies of the optimized adsorbate/substrate system, the adsorbate in the structure, and the clean substrate, respectively. The free energy was calculated using the equation:

$$G=E_{ads}+ZPE-TS$$

where G, Eads, ZPE and TS are the free energy, total energy from DFT calculations, zero point energy and entropic contributions, respectively, where T is set to 300K.

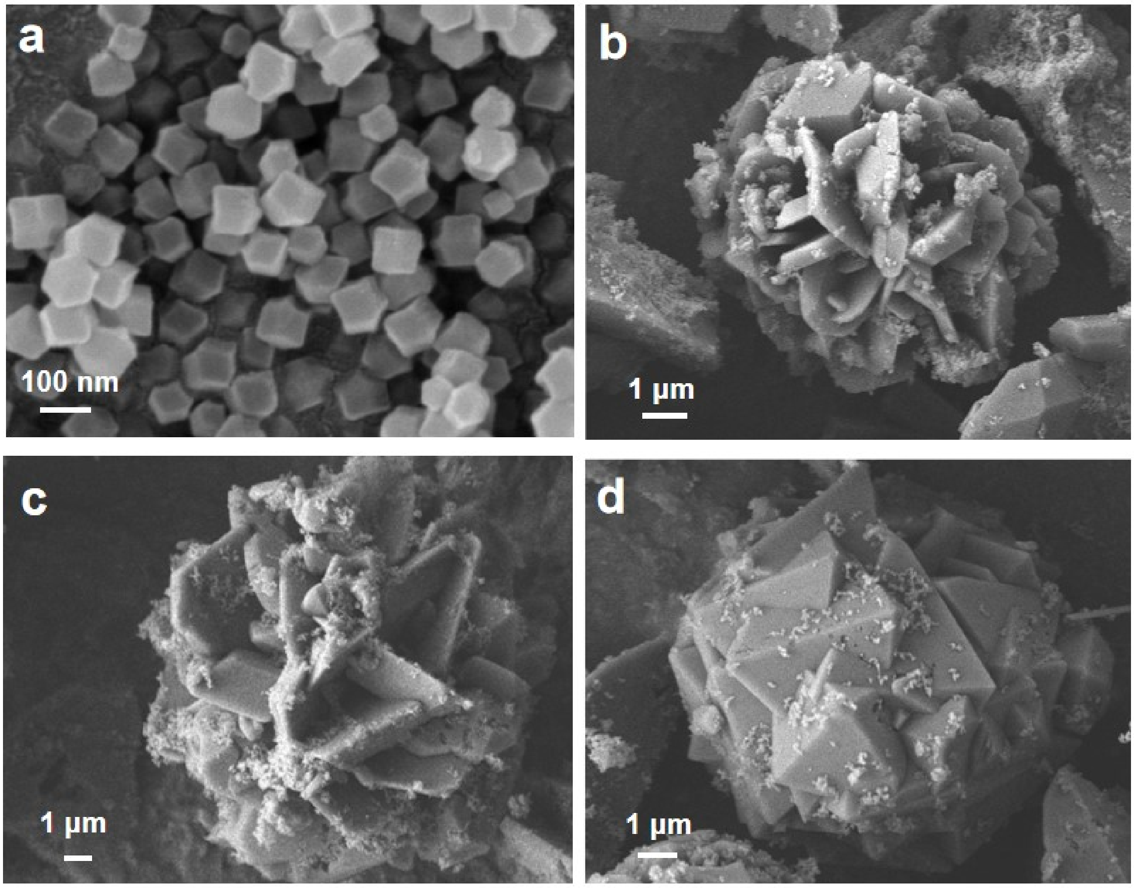

Figure S1. SEM images of (a) Fe-ZIF-8, (B) Fe-ZIF-8-TFTP-1, (c) Fe-ZIF-8-TFTP-2, (d) Fe-ZIF-8-TFTP-3.

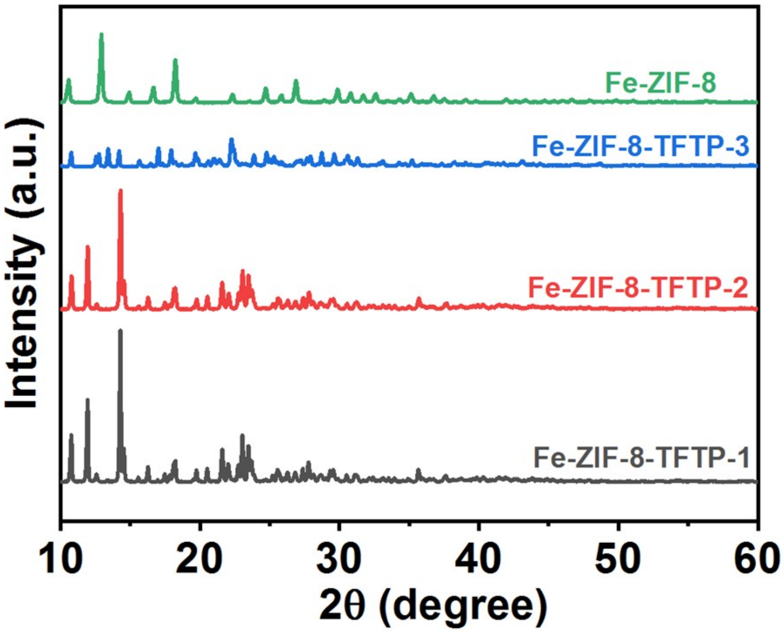

Figure S2. XRD patterns of precursors Fe-ZIF-8-TFTP-1, Fe-ZIF-8- Fe-ZIF-8-TFTP-2, Fe-ZIF-8-TFTP-3 and Fe-ZIF-8.

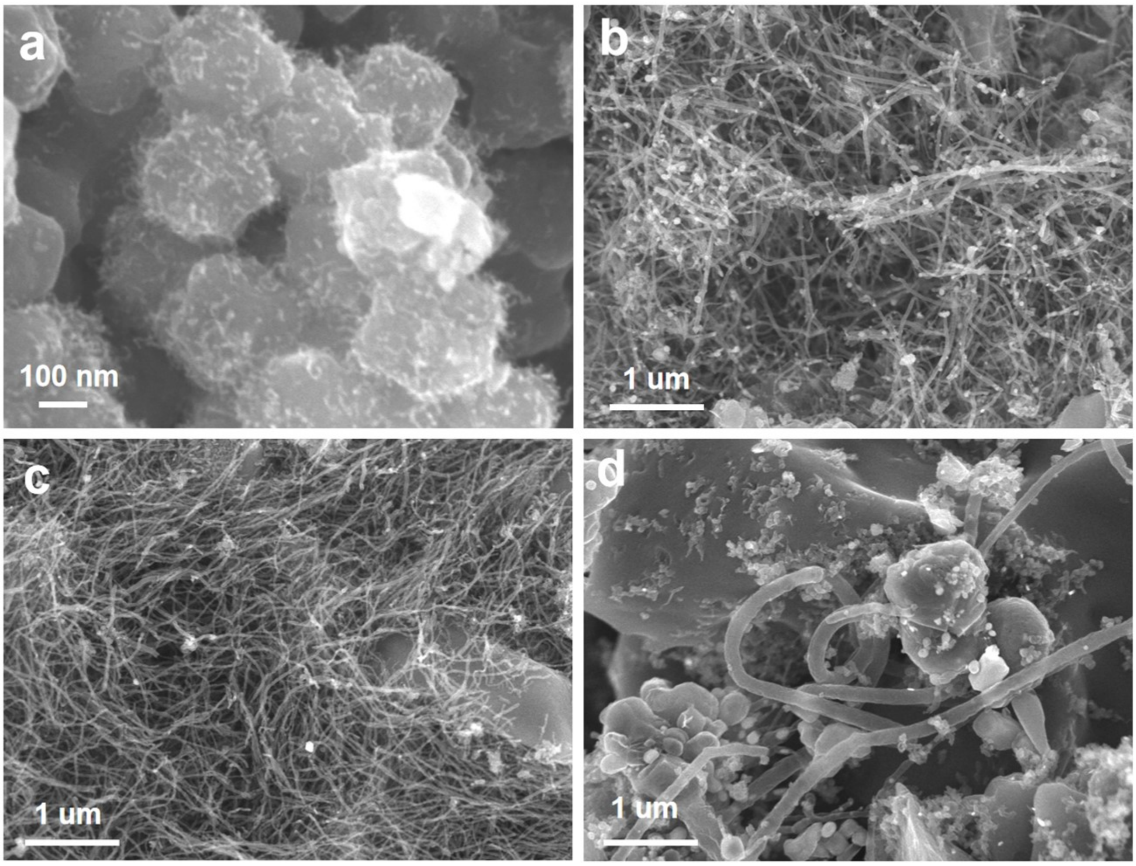

Figure S3. SEM images of (a) Fe-N-CNT, (b) Fe-N/F-CNT-1, (c) Fe-N/F-CNT-2, (d) Fe-N/F-CNT-3.

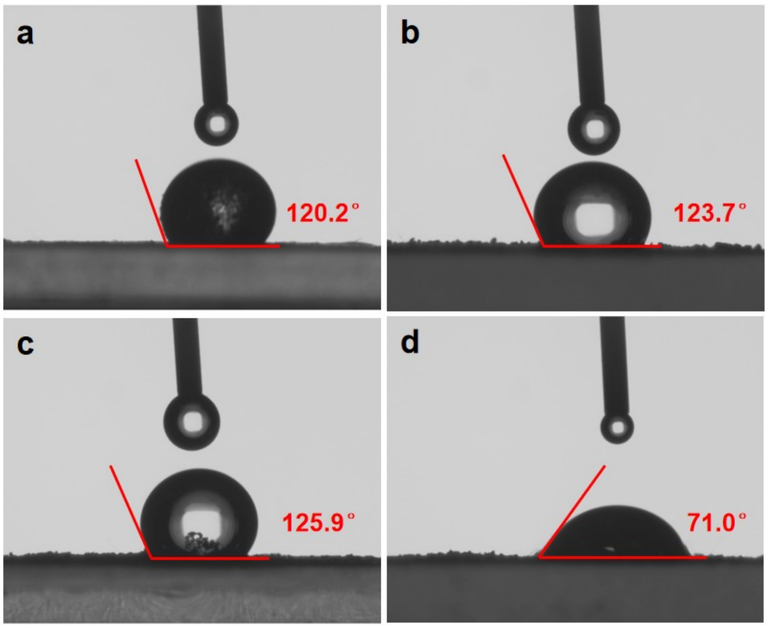

Figure S4. Contact angle of (a) Fe-N/F-CNT-1, (b) Fe-N/F-CNT-2, (c) Fe-N/F-CNT-3 and (d) Fe-N-CNT.

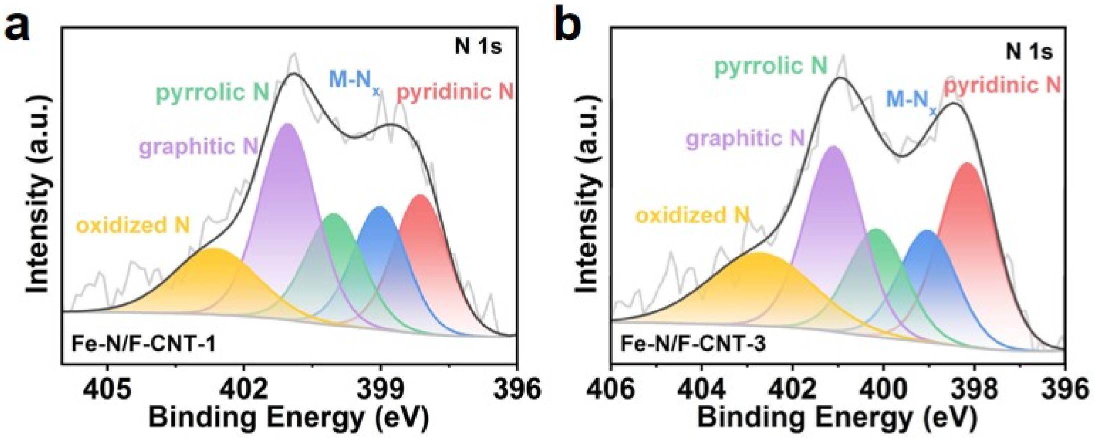

Figure S5. high-resolution XPS spectra of N 1s of (a) Fe-N/F-CNT-1 and (b) Fe-N/F-CNT-3.

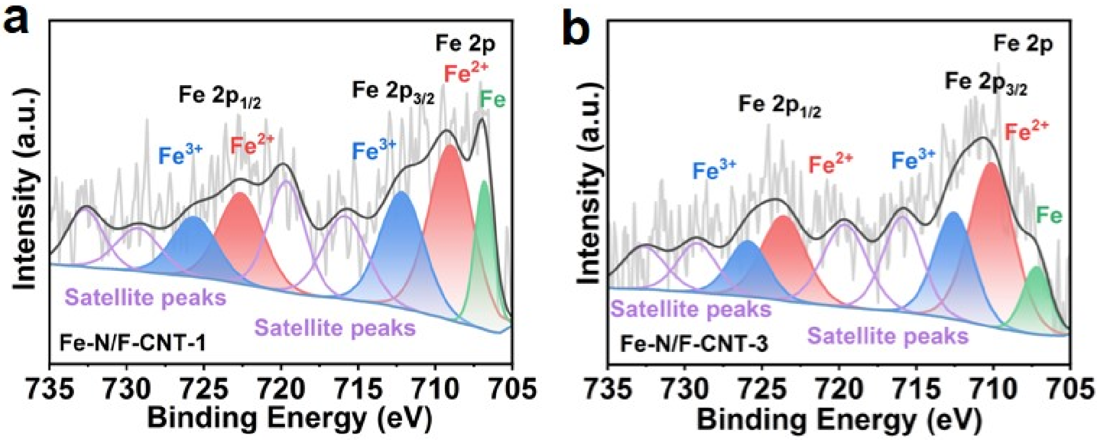

Figure S6. High-resolution XPS spectra of Fe 2p of (a) Fe-N/F-CNT-1 and (b) Fe-N/F-CNT-3.

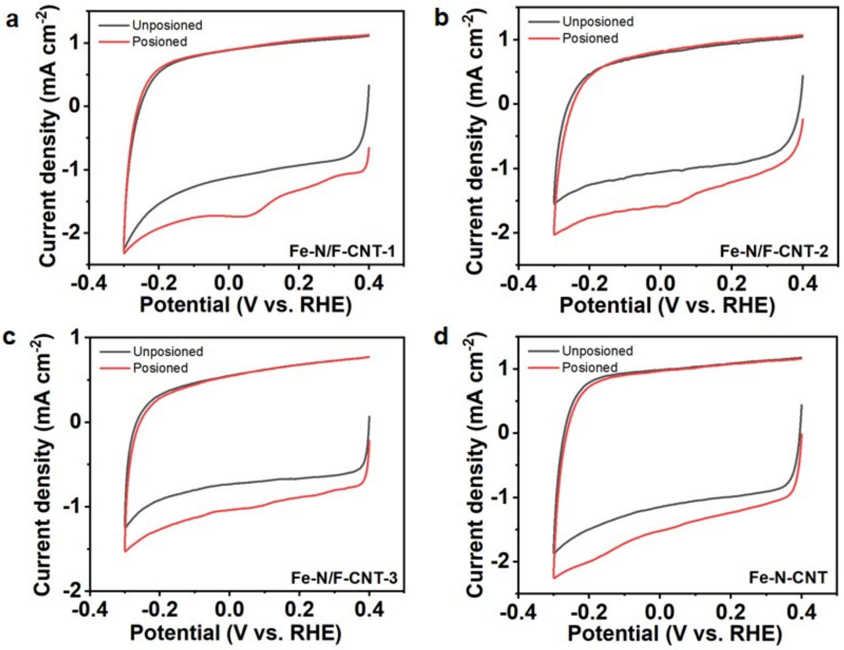

Figure S7. CV curves (10 mV s^{-1}) before and after $NaNO_2$ poisoning procedure in a 0.5 M acetate buffer at pH 5.2. Catalyst loading: 0.51 mg cm^{-2}.

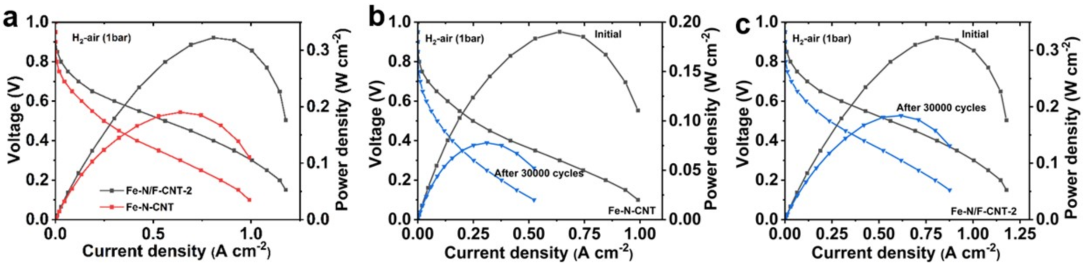

Figure S8. (a) Polarization and power density curves of different catalysts in 1.0 bar H_2/air PEMFC, Polarization and power density curves of (b) Fe-N-CNT and (c) Fe-N/F-CNT-2 cathode catalyst after 30,000 voltage cycles.

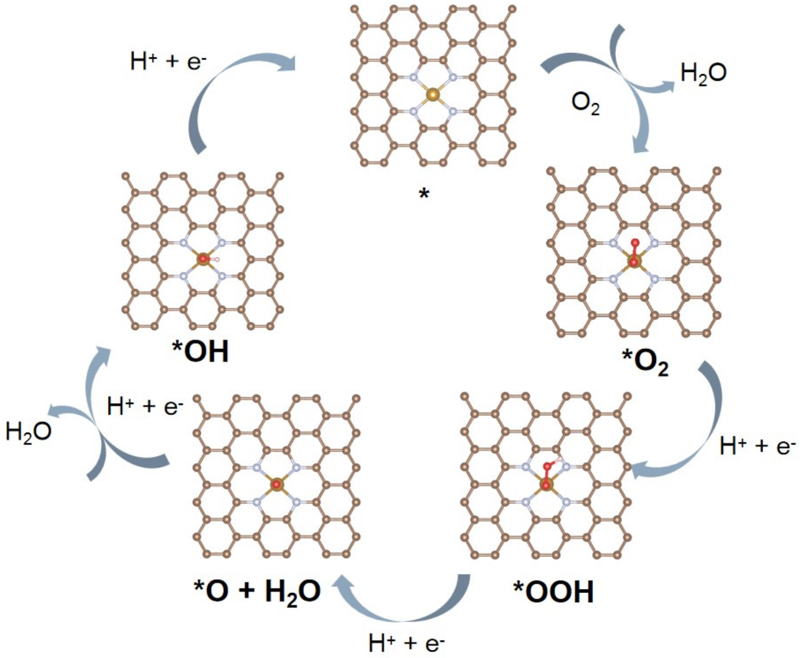

Figure S9. Optimized ORR reaction process of FeN_4.

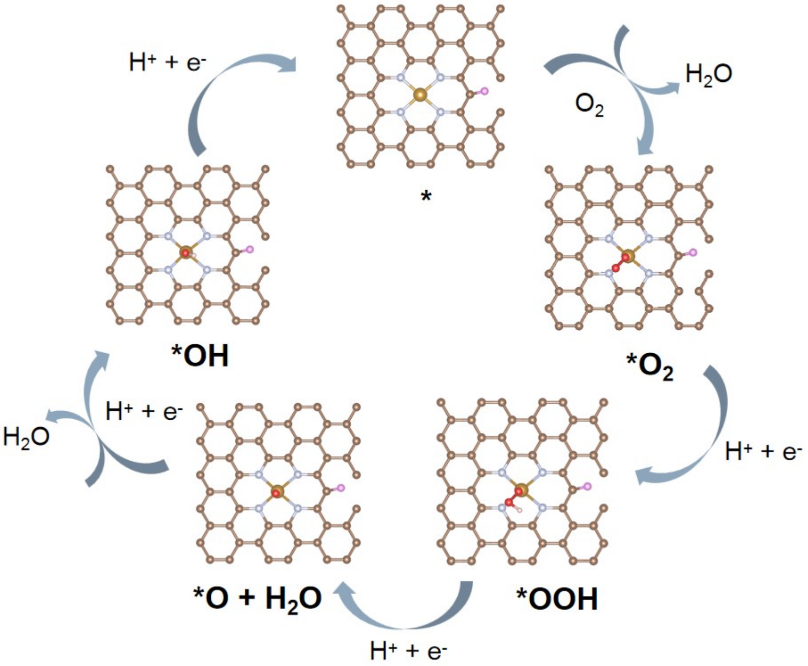

Figure S10. Optimized ORR reaction process of FeN_4-CF.

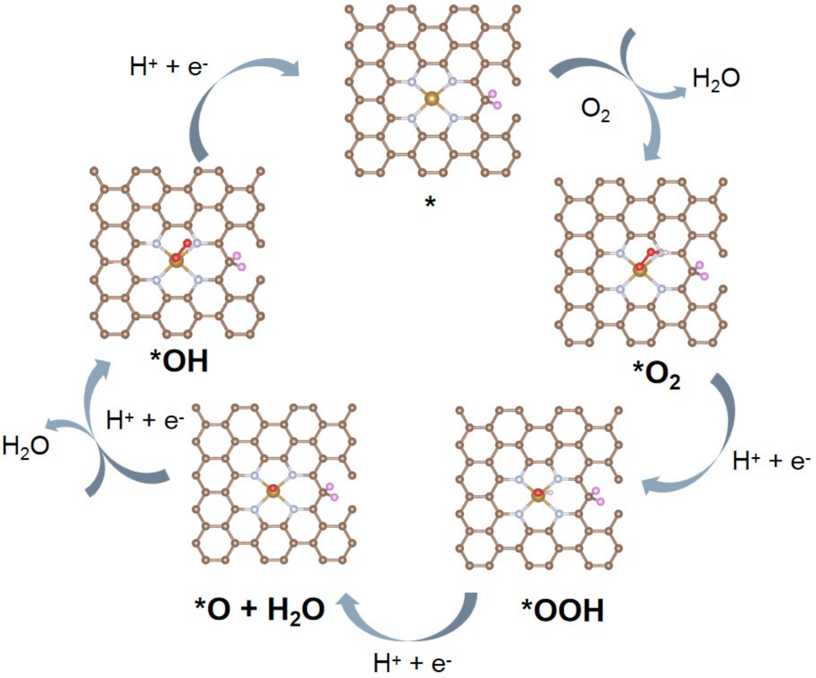

Figure S11. Optimized ORR reaction process of FeN_4-CF_2.

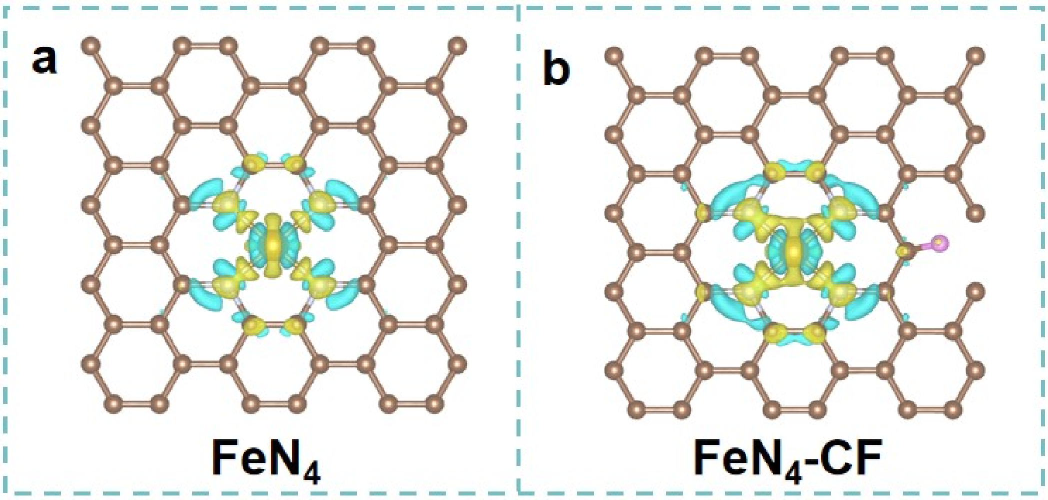

Figure S12. The differential charge density of (a) FeN_4 and (b) FeN_4-CF.

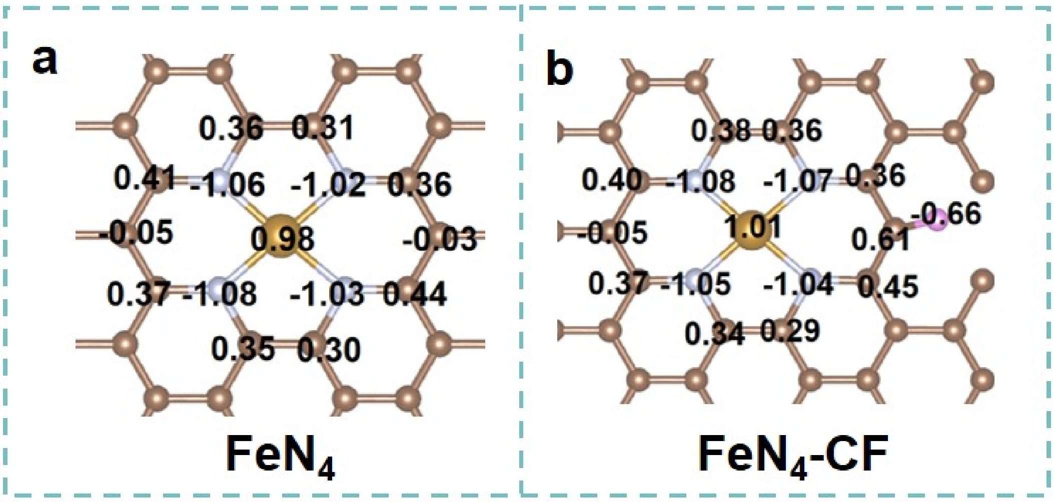

Figure S13. Bader charge distribution of (a) FeN_4 and (b) FeN_4-CF.

Table S1. Textural properties of Fe-N/F-CNT-1, Fe-N/F-CNT-2, Fe-N/F-CNT-3 and Fe-N-CNT catalysts determined by Nitrogen adsorption/desorption isotherms.

Textural property	S_{BET} $[m^2g^{-1}]$	S_{micro} $[m^2g^{-1}]$	S_{meso} $[m^2g^{-1}]$	V_{total} $[cm^3g^{-1}]$	V_{micro} $[cm^3g^{-1}]$	V_{meso} $[cm^3g^{-1}]$	Average Diameter [nm]
Fe-N/F-CNT-1	573.865	162.767	411.098	0.5932	0.070	0.5232	4.135
Fe-N/F-CNT-2	571.773	143.826	427.947	0.5958	0.060	0.5358	4.168
Fe-N/F-CNT-3	775.652	341.954	433.698	0.5137	0.148	0.6617	3.412
Fe-N-CNT	479.458	-	479.458	1.0310	-	1.031	8.602

Table S2. Elemental compositions of Fe-N/F-CNT-1, Fe-N/F-CNT-2, Fe-N/F-CNT-3 and Fe-N-CNT according to XPS measurements.

Samples	C (at. %)	N (at. %)	O (at. %)	F (at. %)	Fe (at. %)
Fe-N/F-CNT-1	89.83	3.46	5.81	0.46	0.45
Fe-N/F-CNT-2	90.72	3.34	4.87	0.47	0.60
Fe-N/F-CNT-3	89.85	3.58	5.68	0.54	0.35
Fe-N-CNT	93.40	2.05	4.29	-	0.26

Table S3. ORR data for Fe-N/F-CNT-1, Fe-N/F-CNT-2, Fe-N/F-CNT-3, Fe-N-CNT and commercialized Pt/C.

Samples	E_{onset} (V)	$E_{1/2}$ (V)	J_L (mA cm^{-2})
Fe-N/F-CNT-1	0.884	0.770	4.81
Fe-N/F-CNT-2	0.893	0.800	4.53
Fe-N/F-CNT-3	0.871	0.745	3.44
Fe-N-CNT	0.876	0.711	4.93
Pt/C	0.917	0.798	5.90

Table S4. ORR data for Fe-N/F-CNT-2 and other reported similar catalysts.

Samples	E_{onset} (V)	$E_{1/2}$ (V)	J_L (mA cm^{-2})	References
Fe-N/F-CNT-2	0.893	0.800	4.53	This work
Fe/S_2-NC	-	0.784	5.30	[8]
Fe-SA-NSC	0.910	0.790	4.87	[9]
FeNC–S–Fe_xC/Fe	-	0.821	5.75	[10]
Cl-Fe-NC	0.94	0.82	-	[11]

References:

1. D. Malko, A. Kucernak and T. Lopes, *Nat. Commun.*, 2016, **7**, 13285.
2. A. Mehmood, M. Gong, F. Jaouen, A. Roy, A. Zitolo, A. Khan, M.-T. Sougrati, M. Primbs, A. M. Bonastre, D. Fongalland, G. Drazic, P. Strasser and A. Kucernak, *Nat. Catal.*, 2022, **5**, 311-323.
3. G. F. l. Kresse, J., *Comput. Mater. Sci.*, 1996, **6**, 15-50.
4. G. F. l. Kresse, J., *Phys. Rev. B*, 1996, **54**, 11169-11186.
5. K. B. John P. Perdew, *Phys.Rev.Lett*, 1996, **77**, 3865-3868.
6. G. J. Kresse, D., *Phys. Rev. B*, 1999, **59**, 1758-1775.
7. P. E. Blöchl, *Phys. Rev. B*, 1994, **50**, 17953−17979.
8. H. Jin, X. Zhao, L. Liang, P. Ji, B. Liu, C. Hu, D. He and S. Mu, *Small*, 2021, **17**, 2101001.
9. Y. Zhou, X. Tao, G. Chen, R. Lu, D. Wang, M. X. Chen, E. Jin, J. Yang, H. W. Liang, Y. Zhao, X. Feng, A. Narita and K. Mullen, *Nat. Commun.*, 2020, **11**, 5892.
10. Y. Qiao, P. Yuan, Y. Hu, J. Zhang, S. Mu, J. Zhou, H. Li, H. Xia, J. He and Q. Xu, *Adv. Mater.*, 2018, **30**, 1804504.
11. P. Sabhapathy, P. Raghunath, A. Sabbah, I. Shown, K. S. Bayikadi, R. K. Xie, V. Krishnamoorthy, M. C. Lin, K. H. Chen and L. C. Chen, *Small*, 2023, DOI: 10.1002/smll.202303598, e2303598.